

CCD *UBVRI* photometry of the open cluster Berkeley 8

Hikmet ÇAKMAK^{1*} , Raúl MICHEL²  and Yüksel KARATAŞ¹ 

¹Department of Astronomy and Space Sciences, Faculty of Science, İstanbul University, 34116, İstanbul, Turkey

²Observatorio Astronómico Nacional, Universidad Nacional Autónoma de México, Apartado Postal 877,
C.P. 22800, Ensenada, B.C., México

Received: ???.?.2019 • Accepted/Published Online: ???.?.2019 • Final Version: ???.?.2019

Abstract: The poorly studied Berkeley 8 (Be 8) open cluster is analysed from CCD *UBVRI* photometric data taken with the 0.90 m telescope at the Sierra Nevada Observatory. The $Z = +0.008$ PARSEC isochrone gave us a reddening of $E(B-V) = 0.69 \pm 0.03$, a distance of 3410 ± 300 pc and an age of 2.8 ± 0.2 Gyr. Its median Gaia DR2 distance, $d = 3676 \pm 810$ pc is in good agreement with our photometric distances, 3410 - 3620 pc within the uncertainties. The kinematic parameters of five likely members of Be 8 with the circular orbits, $ecc = [0.23, 0.30]$ reflect the properties of the Galactic thin disc, which is also consistent with what is expected of its metal content ($[M/H] = -0.27$). Be 8 with $R > 9$ kpc (co-rotation gap at 9 kpc) may have been originating from different galactic radius or different star formation region.

Key words: (Galaxy:) open clusters and associations:general - Galaxy: abundances - Galaxy: evolution

1. Introduction

Open clusters (OCs) are valuable objects for revealing stellar evolution and the structure, chemical and dynamical evolution of the Galactic disk. Be 8 has been studied by Hasegawa et al. (2004) [1] from CCD BVI photometry and by Bukowiecki et al. (2011) [2] from 2MASS JHK_s photometry. Be 8 is located close to a portion of the Perseus spiral arm in the second quadrant of the Galaxy (Figure 1), according to its equatorial and Galactic coordinates (WEBDA) [3] (rows 1–4 of Table 1). The main aim of this paper is to present astrophysical parameters such as reddening, distance and age of Be 8 from four colour indices, $(B - V)$, $(V - I)$, $(R - I)$ and $(G_{BP} - G_{RP})$ obtained from deep CCD *UBVRI* and Gaia photometries. This kind of data is also valuable for classifying early-type stars, Blue Stragglers (BS) and Red Giant/Red Clump (RG/RC) candidates in the colour magnitude diagrams (CMDs), and thus probable candidates are proposed for future spectroscopic observations. We used Gaia DR2 astrometric data (proper motion components and parallaxes) [4, 5] and Gaia DR2 photometry ($G - G_{BP} - G_{RP}$) for determining the probable members of Be 8. With the Gaia DR2 astrometric data, a membership method was done in the literature [6–8]. The membership determinations of previous works have been based on the proper motions of Roeser et al. (2010) [9] in combination with the 2MASS JHK_s photometry of Skrutskie et al. (2006) [10]. Cantat-Gaudin et al. (2018) [11] state that the proper motion uncertainties of UCAC4 fall in the range of 1–10 mas yr^{−1} [9, 12]. According to Lindegren et al. (2018) [4] and Brown et al. (2018) [5], the mean parallax errors of Gaia DR2 catalogue fall in the range 0.02–0.04 mas for $G < 15$ and 0.1

*Correspondence: hcakmak@istanbul.edu.tr

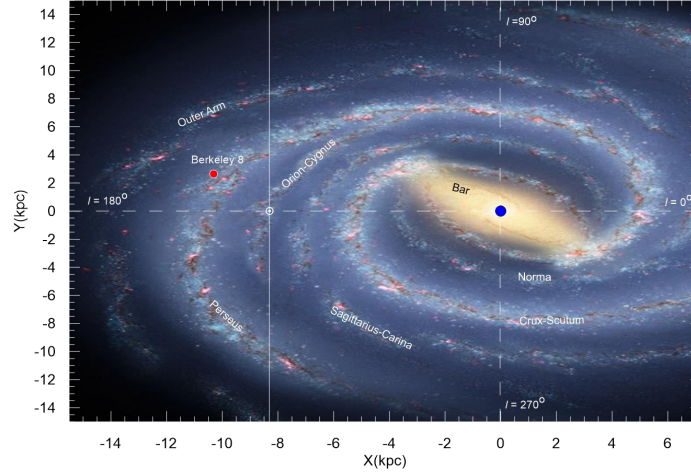


Figure 1. Spatial distribution (X, Y) (kpc) (filled red circle) of Be 8. See Section 6 for the estimation of (X, Y) values. The sun is at $R_{\odot} = 8.2 \pm 0.1$ kpc [34]. The image is adapted from the image¹ credit by Robert Hurt, IPAC; Bill Saxton, NRAO/AUI/NSF.

Table 1. Rows (1)-(4) mean the central equatorial (J2000) and the Galactic coordinates of WEBDA. Air mass and exposure times (s) of filters are listed in rows 5–10.

Cluster	Be 8
α_{2000} (h m s)	02 01 08.00
δ_{2000} ($^{\circ}$ ' '')	+75 29 38.25
ℓ ($^{\circ}$)	127.35
b ($^{\circ}$)	+13.21
Air mass	1.276 – 1.280
Filter U Exp.Time (s)	9, 90, 3x300
Filter B Exp.Time (s)	5, 50, 500
Filter V Exp.Time (s)	3, 30, 300
Filter R Exp.Time (s)	2, 20, 200
Filter I Exp.Time (s)	2, 20, 200

mas for $G < 17$, whereas the uncertainties of proper motion components are up to 0.06 mas yr^{-1} for $G < 15$ mag and 0.2 mas yr^{-1} for $G < 17$.

This paper is organised as follows: Section 2 describes the observation and reduction techniques. Its dimensions are given in Section 3. Section 4 is devoted for the classification of cluster members. Section 5 describes the derivation of the astrophysical parameters. The classification of BS and RG/RC candidates and its morphological age determination are presented in Section 6. Section 7 focuses into its kinematics and orbital parameters. Discussions and Conclusions are given in Section 8.

2. Observations and Reduction techniques

Observations of Be 8 were carried out, during the photometric night of December 3 2015, with the 0.90m (f/8 Ritchey-Chrétien) telescope at Sierra Nevada Observatory (Granada, Spain). A filter wheel with *UBVRI* filters

¹<https://www.universetoday.com/102616/our-place-in-the-galactic-neighborhood-just-got-an-upgrade>

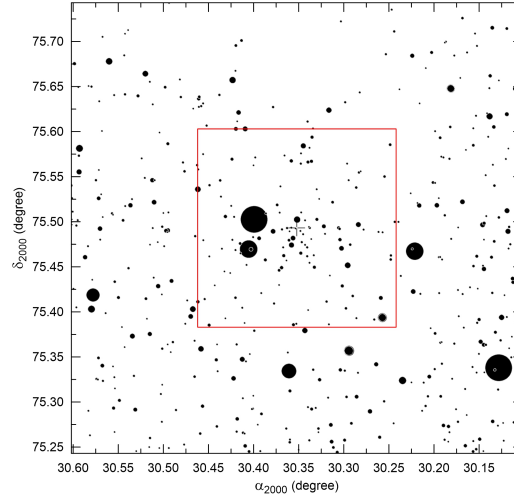


Figure 2. The image of Be 8 for a region of $18.3' \times 17.2'$ (<https://www.aavso.org> (AAVSO)). The red rectangle indicates the field of view of the SNO detector, $13.2' \times 13.2'$.

and a scientific grade Marconi-EEV CCD42-40 were employed. The CCD is a 2048×2048 $13.5\text{-}\mu\text{m}$ square-pixel detector with a nominal gain of $1.35\text{ e}^-/\text{ADU}$ and a readout noise of 7.14 e^- at the 2×2 binning employed. Along with the optics, it covers a field of view of $13.2 \times 13.2\text{ arcmin}^2$. Apart from Be 8, other open clusters and some Landolt standard fields [13] were observed. Flat fields were also acquired at the beginning of the night and many bias frames were also taken.

The data reduction was carried out by R. Michel² using the IRAF³ package and together with some home-made auxiliary Fortran programs and Awk scripts. All the images were bias subtracted and flat-field corrected (CCDRED). Cosmic rays were removed with the L.A. Cosmic⁴ script van Dokkum (2001) [14].

The standard magnitudes were taken from the catalogue by Landolt (2009) [13] and supplemented with the secondary photometric standards by Cutri et al. (2013) [15]. As a result, the transformation coefficients were found (FITPARAMS). For magnitude estimation, transformation equations used are

$$M_\lambda = m_\lambda - (k_1 - k_2C)X + \eta_\lambda C + \zeta_\lambda \quad (2.1)$$

where m_λ , k_1 , k_2 , C and X are observed instrumental magnitude, primary and secondary extinction coefficients, colour index and air mass, respectively. M_λ , η_λ , ζ_λ are standard magnitude, atmospheric extinction-corrected instrumental magnitude, transformation coefficient and photometric zero point, respectively. The other details of data reduction can be found in the papers of Akkaya et al. (2010) [16] and Akkaya et al. (2015) [17]. Air-mass range and exposure times in each band during the observations are given in rows 5–10 of Table 1.

Figure 2 presents the finding chart⁵ of Be 8 ($18.3' \times 17.2'$). The red rectangle indicates the field of view of the SNO detector, $13.2' \times 13.2'$. The photometric errors in V and $(R - I)$, $(V - I)$, $(B - V)$, $(U - B)$ of

²Data may be requested from R. Michel.

³IRAF is distributed by the National Optical Observatories, operated by the Association of Universities for Research in Astronomy, Inc., under cooperative agreement with the National Science Foundation.

⁴<http://www.astro.yale.edu/dokkum/lacosmic>

⁵Obtained from <https://www.aavso.org> (AAVSO) web page, [accessed 09 June 2019]

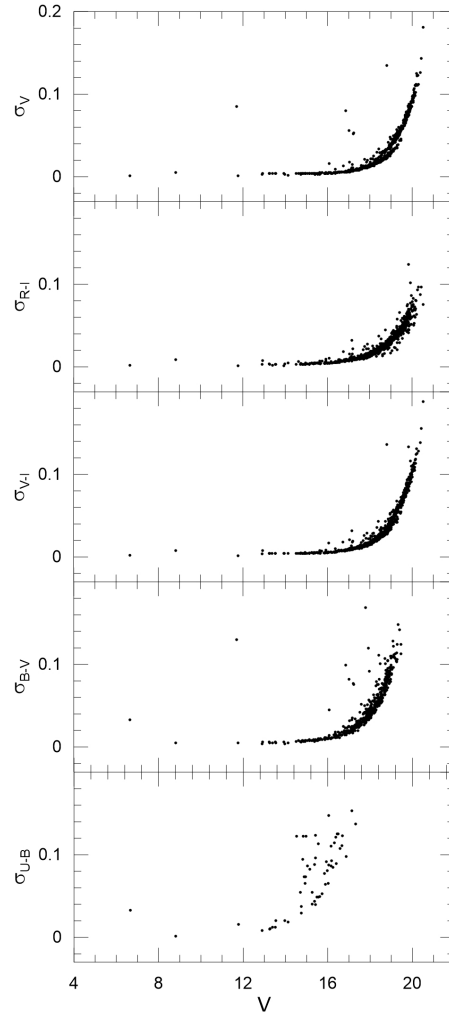


Figure 3. Photometric errors of the V apparent magnitude and four colours against the V magnitude for Be 8.

Table 2. The mean photometric errors of V , $(U - B)$, $(B - V)$, $(R - I)$, $(V - I)$ of Be 8.

V	σ_V	σ_{U-B}	σ_{B-V}	σ_{R-I}	σ_{V-I}	N
6 - 13	0.017	0.014	0.031	0.004	0.004	6
13 - 14	0.004	0.014	0.005	0.003	0.004	7
14 - 15	0.004	0.074	0.007	0.004	0.004	13
15 - 16	0.004	0.071	0.009	0.005	0.005	30
16 - 17	0.007	0.104	0.018	0.007	0.009	50
17 - 18	0.011	0.145	0.034	0.012	0.015	166
18 - 19	0.022	-	0.063	0.023	0.027	265
19 - 20	0.058	-	0.110	0.047	0.066	216
20 - 21	0.107	-	-	0.073	0.117	30

Be 8 are presented in Figure 3. Its mean photometric errors are also listed in Table 2. Our inspection of Figure 3 and Table 2 indicates that stars brighter than $V = 18$ have errors smaller than 0.03 in $(R - I)$, $(V - I)$, $(B - V)$. For $V > 20$, the errors in $(R - I)$ and $(V - I)$ are larger than 0.03. After $V > 18$, the errors in $(B - V)$ are up to $\approx 0^m.03$. The errors in $(U - B)$ are less than 0.01 for $V < 14$, whereas for $14 < V \leq 18$, large errors increase.

3. Dimensions of Be 8

The stellar radial density profile (RDP) of Be 8 (Figure 4) has been built from Gaia DR2 photometry for the equatorial coordinates (Table 1). Its RDP have been constructed by counting stars in concentric rings of increasing width with distance to its centre. We choose $\Delta R = 15.0'$ as the wide external ring of the stellar comparison field. As emphasised by Bonatto and Bica (2007) [18], the number and width of rings were optimised so that the resulting RDP had adequate spatial resolution with moderate 1σ Poisson errors. The solid curve (Figure 4) denotes the fitted King's profile [19]. Here we adopt the two-parameter function, $\sigma(R) = \sigma_{bg} + \sigma_0 / (1 + (R/R_c)^2)$, where σ_{bg} is the residual background density, σ_0 the central density of stars, and R_{core} the core radius. The horizontal red bar shows the stellar background level measured in the comparison field, and the 1σ profile fit uncertainty is shown by the shaded region. The core and cluster radii from Figure 4 have been determined as $R_{core} = 1.8'$ and $R_{RDP} = 15.0'$, respectively. These dimensions are quite close to the ones of $(R_{core}, R_{RDP}) = (1.52', 15.5')$ of Bukowiecki et al. (2011) [2].

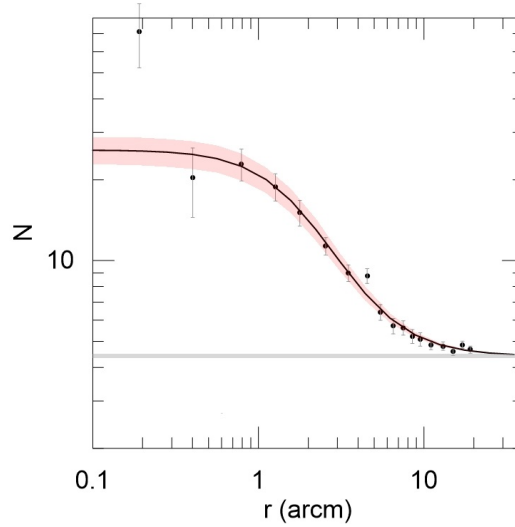


Figure 4. Stellar RDP (filled dots) of Be 8. Solid line shows the best-fit King profile. Horizontal red bar: stellar background level measured in the comparison field. Shaded region: 1σ King fit uncertainty. The core and cluster radii are obtained as $R_{core} = 1.8'$ and $R_{RDP} = 15.0'$, respectively.

4. Classification of cluster members

For the membership determination of Be 8, our CCD $UBVRI$ photometric data have been matched with Gaia DR2 astrometric (proper motion components and parallaxes) (μ_α , μ_δ and ϖ) and Gaia DR2 photometric data. The μ_α versus μ_δ ($mas\ yr^{-1}$) for all stars of Be 8 (filled dots) is shown in Figure 5. Grey dots denote the field stars inside $R = 15'.0$ arcmin centred on Be 8. We have applied Gaussian Mixture method for all stars of Be 8.

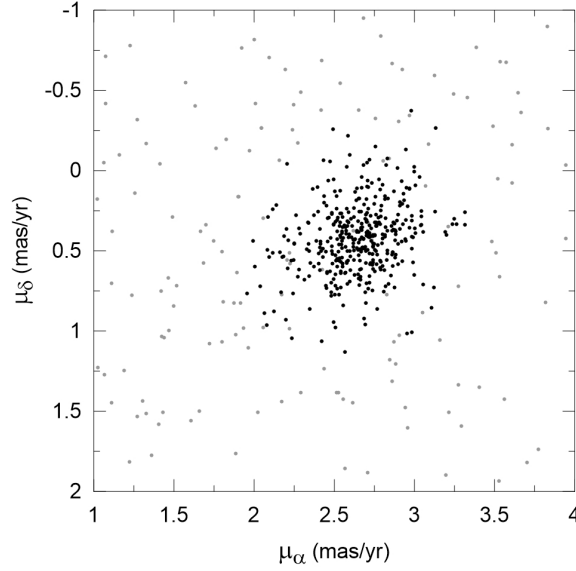


Figure 5. The μ_α versus μ_δ for Be 8 (filled stars). Small grey dots represent the Gaia DR2 astrometric data for a $15'.0$ field centred on Be 8.

By applying Gaussian Mixture Model (GMM) [20] to the stars in the cluster region of Be 8, we have determined the membership probability (P). The model considers that the distribution of proper motions of the stars in a cluster's region can be represented by two elliptical bivariate Gaussians, by following Wu et al. (2002) [21] which include the proper motion's errors in the frequency function. The expressions used can be found in the papers of Balaquer-Nunez et al. [6], Sariya et al. (2012) [7] and Dias et al. (2018) [8]. P is defined Φ_c / Φ . Here $\Phi = \Phi_c + \Phi_f$ is the total probability distribution. c and f subscripts for cluster and field parameters, respectively. The used parameters for estimation of Φ_c and Φ_f are μ_α , μ_δ , ϖ , σ_{μ_α} , σ_{μ_δ} , σ_ϖ . The averages and their uncertainties of proper motion components and parallaxes in the distributions of the cluster and field regions in Figure 5 are listed in Table 3. Figure 6(a) shows the membership probability (P) histogram, which provides a very clear separation between cluster and field stars. The number of stars with membership probability which is greater than 90% is 273. These likely members have been considered for deriving astrophysical parameters of Be 8. From the relation of the membership probability (P) versus G mag (Figure 6(b)), high membership probability appears to extend down to $G \sim 21$ mag.

Table 3. The medians and their uncertainties of proper motion components (μ_α , μ_δ) ($mas\ yr^{-1}$) and parallaxes (ϖ) (mas) from the distributions of the cluster and field regions on Figure 5.

	$\mu_\alpha \pm \sigma_{\mu_\alpha}$	$\mu_\delta \pm \sigma_{\mu_\delta}$	$\varpi \pm \sigma_\varpi$
Cluster region	2.648 ± 0.24	0.421 ± 0.23	0.266 ± 0.12
Field region	0.33 ± 2.23	0.347 ± 1.75	0.545 ± 0.45

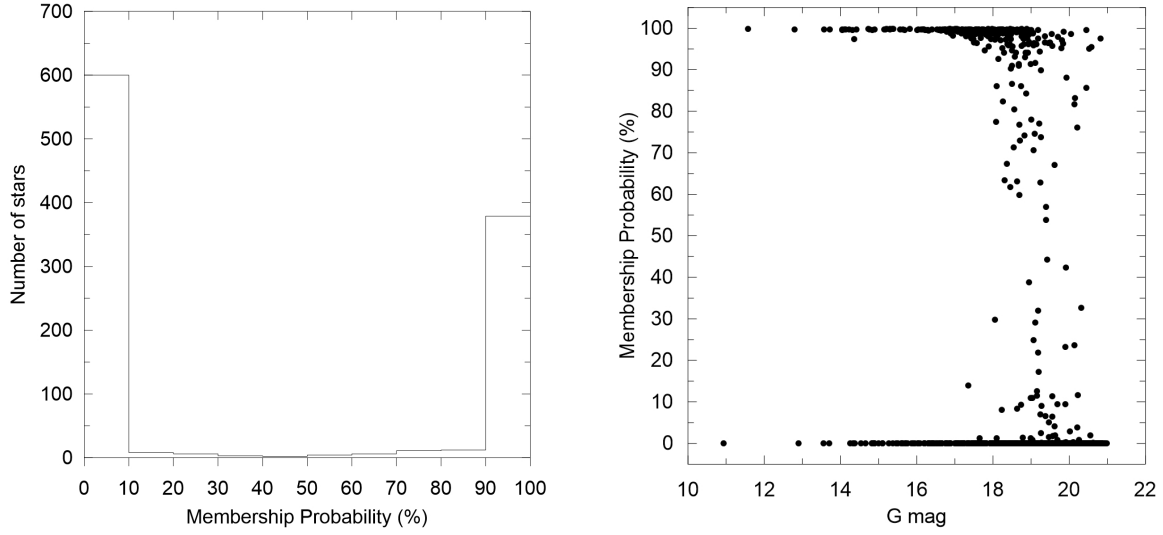


Figure 6. The membership probability histogram $P(\%)$ (left panel) and $P(\%)$ versus G mag (right panel) for all stars of Be 8.

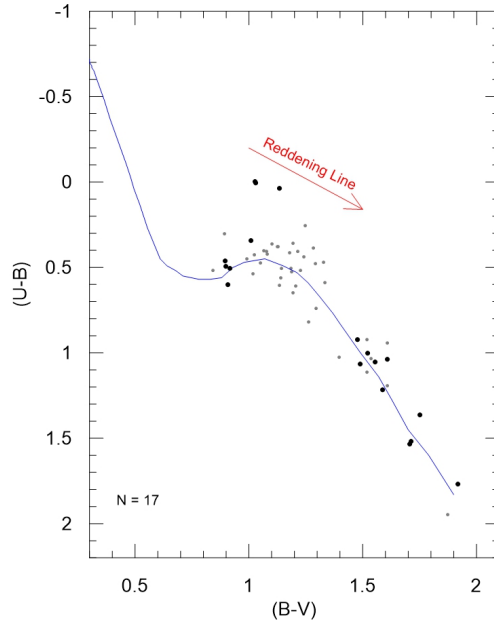


Figure 7. $(U - B) - (B - V)$ two colour diagram for the 17 likely members (filled dots) of Be 8. The dashed blue line represents the Schmidt-Kaler (SK82) main-sequence. Field stars are shown with small grey dots. Red arrow denotes the reddening.

5. Astrophysical parameters of Be 8 open cluster

The two colour $(U - B) - (B - V)$ (CC) diagram of the 17 probable members for Be 8 is displayed in Figure 7. The blue line denotes the reddened main sequence for dwarfs and red giants of Schmidt-Kaler (1982)(SK82) [22]. It appears from Fig. 7 that Be 8 contains F-type stars which are quite valuable for determining photometric metal abundance, $[M/H]$. These F type stars with $(U - B) < 0.35$ and $0.9 < (B - V) < 1.2$ have large UV-

Table 4. The derived fundamental astrophysical parameters of Be 8 for four colour indices.

Colour	$(V_0 - M_V)$	d (kpc)	$\log(A)$	A (Gyr)
$(B - V)$	12.66 ± 0.19	3.41 ± 0.30	9.45 ± 0.03	2.80 ± 0.20
$(V - I)$	12.67 ± 0.31	3.42 ± 0.49	9.45 ± 0.03	2.80 ± 0.20
$(R - I)$	12.79 ± 0.32	3.62 ± 0.53	9.45 ± 0.03	2.80 ± 0.20
$(G_{BP} - G_{RP})$	12.71 ± 0.31	3.48 ± 0.50	9.45 ± 0.03	2.80 ± 0.20

excesses, $\delta(U - B) = 0.15 - 0.48$. A member star with $\delta(U - B) = 0.15$ estimates $[M/H] = -1.0$, which is very poor for Galactic open clusters. The other three members with $\delta(U - B) = 0.47 - 0.48$ do not allow us to determine a reasonable $[M/H]$ value, due to their large UV-excesses which are insensitive to the metal abundance calibration (see the paper of Karataş and Schuster (2006) [23]). Moreover, their photometric errors in $(U - B)$ are larger at a level of $\sigma_{(U-B)} = 0.10 - 0.15$.

Since these issues make it difficult to determine its photometric metal abundance and reddening from CC diagram, we have derived the reddenings, distance moduli and ages of Be 8 from the PARSEC isochrones of Bressan et al. (2012) [24] on the CMDs for four colour indices. The appropriate PARSEC isochrones for different heavy element abundance mass fractions ($Z = +0.015, +0.004, +0.008$) (left panel of Figure 8) and reddenings have been fitted on the CMDs. The 2.8 Gyr PARSEC isochrones for $Z = +0.008$ abundance gave us a good fit

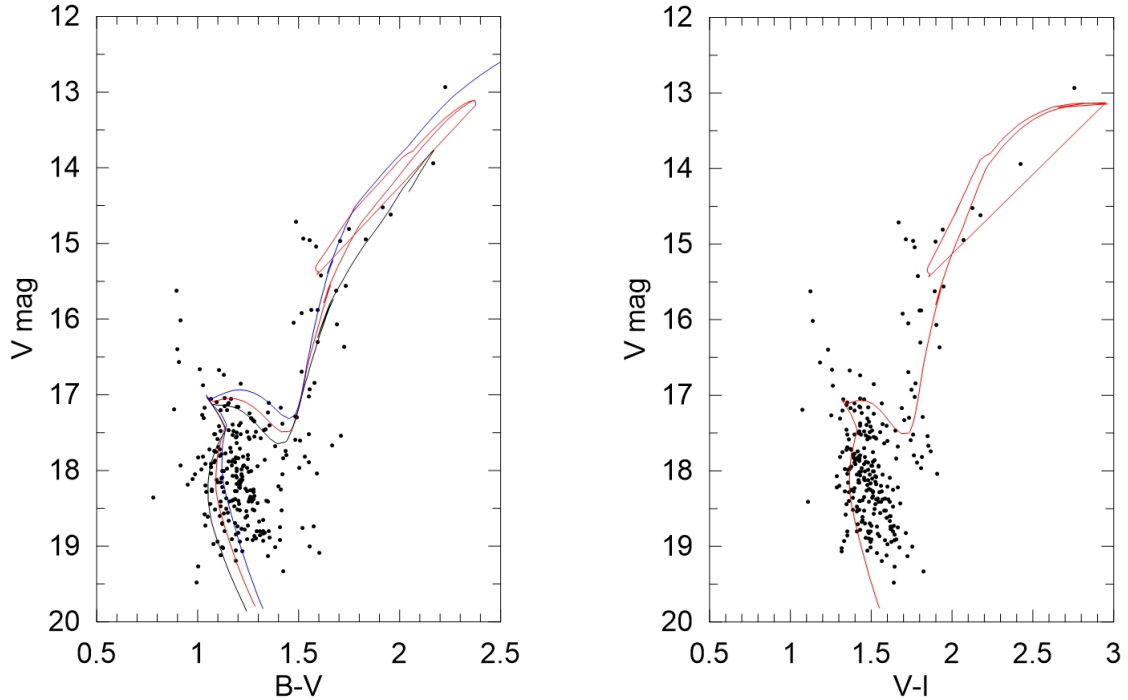


Figure 8. For the 268 likely members of Be 8, CMDs of $V - (B - V)$ (Left) and $V - (V - I)$ (Right). Red curves show the PARSEC isochrones interpolated to $Z = +0.008$. In Left figure the fitted isochrones $Z = +0.015$ (blue line) and $+0.004$ (black line) are also plotted (See Section 5).

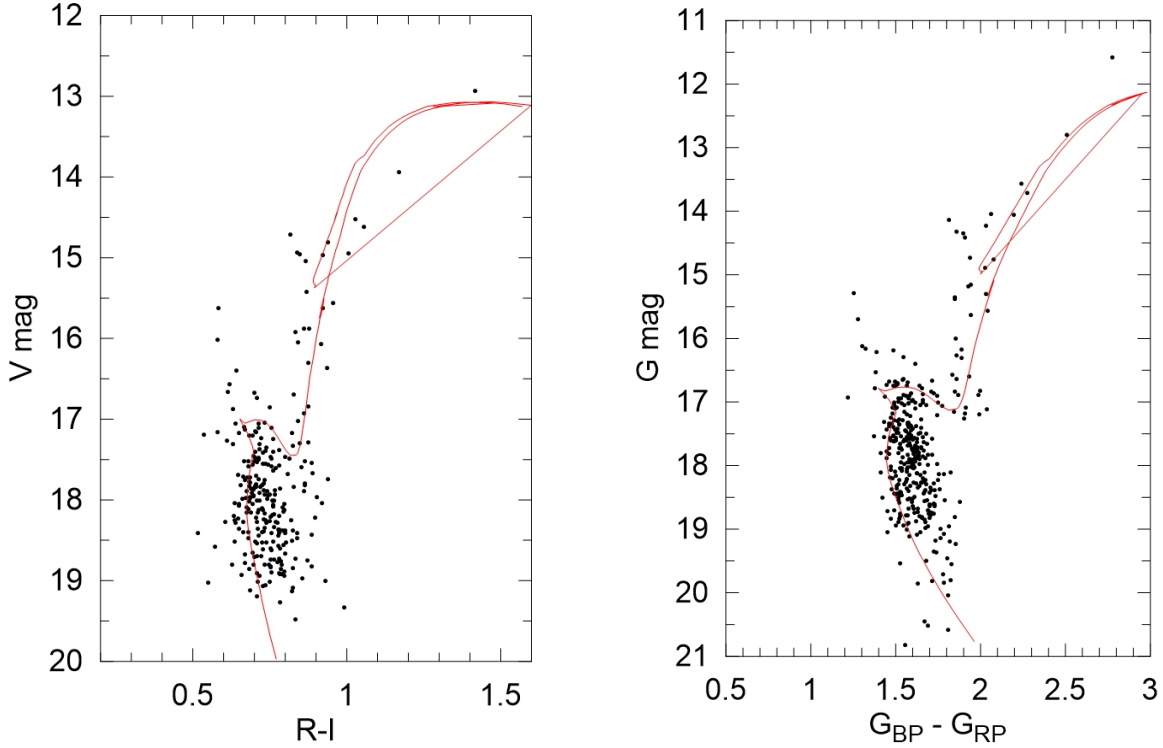


Figure 9. For the 268 likely members of Be 8, CMDs of $V - (R - I)$ (Left) and $G - (G_{BP} - G_{RP})$ (Right). The meanings of the symbols are the same as Figure 8.

solution on the CMDs: $V - (B - V)$, $V - (V - I)$, $V - (R - I)$, $G - (G_{BP} - G_{RP})$ (Figs. 8–9). The equation $Z = Z_{\odot} 10^{[M/H]}$ estimates its photometric metal abundance as $[M/H] = -0.27$. Here the solar heavy metal content is adopted as $Z_{\odot} = +0.015$. The isochrone is varied until a satisfactory fit to the data has been obtained through the observed main-sequence (MS), turn-off (TO), sub-giant (SG) and Red Giant/Red Clump (RG/RC) sequences on the CMDs, as we followed in the papers of Akkaya et al. (2010) [16], Akkaya et al. (2015) [17] and Güneş et al. (2012) [25]. Because of the presence of binaries, the PARSEC isochrones have been shifted to the left and below of MS on all CMDs. The vertical shift gives the (true) distance modulus, $DM = (V_0 - M_V)$. For its age (A , $\log(A)$), the PARSEC isochrones have been shifted both vertically and horizontally on the CMD's with the expression $M_V + 3.1E(B - V) + DM$, for the vertical displacement and $C_0(\lambda_1 - \lambda_2) + E(\lambda_1 - \lambda_2)$, for the horizontal, where λ denotes the wavelengths of $BVR I$ and G , G_{BP} , G_{RP} filters. Here C_0 means de-reddened colour index. The obtained reddenings from four CMDs are $E(B - V) = 0.69 \pm 0.08$, $E(V - I) = 0.87 \pm 0.10$, $E(R - I) = 0.44 \pm 0.05$, $E(G_{BP} - G_{RP}) = 0.91 \pm 0.10$, respectively. Its distance moduli $(V_0 - M_V)/$ distances (d (kpc)) and age (Gyr) for four colours are presented in Cols. 2–5 of Table 4. In order to de-redden the distance moduli (Col. 2 of Table 4) for the colour indices $(V - I)$, $(R - I)$, $(G_{BP} - G_{RP})$, our colour excesses $E(V - I)$, $E(R - I)$ and $E(G_{BP} - G_{RP})$ have been converted from the relations $E(V - I) = 1.25 E(B - V)$, $E(R - I) = 0.69 E(B - V)$ [26–28] and $E(B - V) = 0.775 E(G_{BP} - G_{RP})$ [29].

6. Blue Stragglers, Red Giants/Clumps and Morphological age index

From Figs. 8 – 9 we note that six probable Blue Straggler (BS) candidates lie on $(B - V) < 1.1$, $(V - I) < 1.4$, $(R - I) < 0.7$ for $V < 17.0$, whereas they occupy the region with $G < 16.75$ and $G_{BP} - G_{RP} < 1.4$. BS candidates blur the main-sequence turn off (TO) to a brighter magnitude. RG/RC candidates populate well the red-giant branch (Figs. 8 – 9). These RG/RC stars in old clusters are numerous and luminous as expected. BS (blue plus symbol) and RG/RC (red plus) candidates with $P > 90\%$ have been placed on the nested circles of Figure 10. Two BS candidates reside in core radius of $1.8'$ of Be 8. Four BS stars occupy the inner regions. 26 RG/RC candidates remain within the cluster radius ($R_{RDP} = 15.0'$). Their median Gaia DR2 distances are $d = 3953 \pm 750$ pc ($\varpi = 0.253 \pm 0.048$ mas) (six BS) and $d = 4049 \pm 610$ pc ($\varpi = 0.247 \pm 0.037$ mas) (26 RG/RC), respectively, which are in reasonable agreement with the photometric ones within the uncertainties (Table 4). However, spectroscopic observations of these candidates are needed for their membership confirmation.

The CMDs of Be 8 exhibit noticeable TO and RG/RC sequences (Figs. 8 – 9). By utilising the definition of the morphological age index (MAI), $\delta 1 = (B - V)_{TO} - (B - V)_{RG}$ given by Phelps et al. (1994) [30], we measured $V_{TO} = 17.07$, $(B - V)_{TO} = 1.066$ and $(B - V)_{RG} = 1.599$ on $V - (B - V)$ diagram (left panel of Figure 8). These values estimate $\delta 1 = 0.533$. Here $\delta 1$ is the difference in the colour indices between the bluest point of TO and the colour at the base of RG branch one magnitude brighter than the TO luminosity. Our $\delta 1$ value has been transformed into δV via the equation of $\delta V = 3.77 - 3.75\delta 1$ of Phelps et al. (1994) [30]. Its morphological age has been estimated as $\log A = 9.45$ ($A = 2.94$ Gyr) from the equation, $\log A = 0.04\delta V^2 + 0.34\delta V + 0.07[Fe/H] + 8.76$ of Salaris et al. (2004) [31], applying its the metal abundance ($[M/H] = -0.27$) and $\delta V = 1.771$. Here we assume $[Fe/H] \approx [M/H]$. Its MAI age (2.94 Gyr) is in good compatible with its isochrone age, 2.80 Gyr.

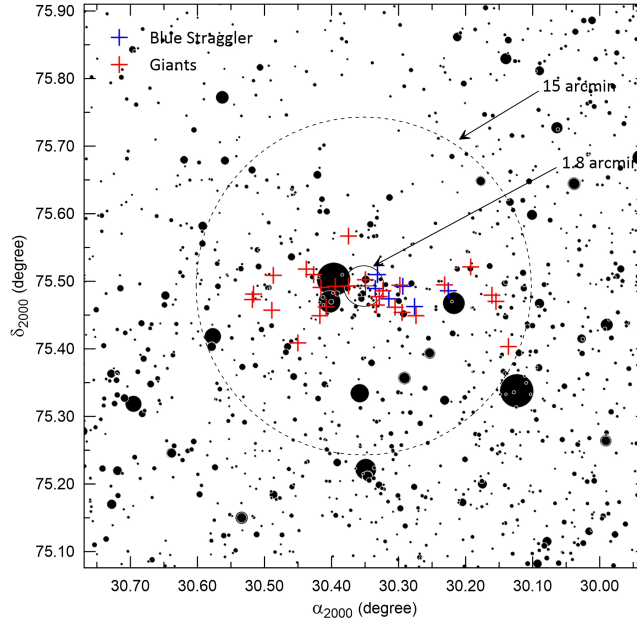


Figure 10. The circles have been drawn for the radii of $1.8'$ and $15.0'$ arc min on the α_{2000} versus δ_{2000} of Be 8. Red and blue pluses represent the RG/RC and BS candidates on the CMDs (Figs. 8 – 9).

Table 5. For five likely members with Gaia DR2 radial velocity data (V_{rad}) km s^{-1} (Col. 8), Gaia DR2 proper motion components mas yr^{-1} (Cols. 6 – 7) and parallaxes (mas) (Col. 9). Their equatorial coordinates (J2000) (Cols. 2 – 3) and V and $(B - V)$ (Cols. 4 – 5). Probability membership value (last column).

STAR-ID	RA	DEC	V	$(B - V)$	$\mu_{\alpha} \pm \sigma_{\mu_{\alpha}}$	$\mu_{\delta} \pm \sigma_{\mu_{\delta}}$	$V_{rad} \pm \sigma_V$	$\varpi \pm \sigma_{\varpi}$	P(%)
508	30.3497	75.5020	12.932	2.226	2.716 ± 0.064	0.397 ± 0.066	-28.05 ± 3.20	0.239 ± 0.040	99.77
862	30.1545	75.4700	13.936	2.165	2.476 ± 0.048	0.420 ± 0.051	-26.40 ± 0.78	0.257 ± 0.032	99.66
737	30.2315	75.4944	14.520	1.918	2.643 ± 0.040	0.484 ± 0.039	-28.55 ± 0.84	0.302 ± 0.024	99.73
299	30.5162	75.4812	14.615	1.956	2.483 ± 0.041	0.500 ± 0.041	-30.88 ± 0.92	0.273 ± 0.025	99.67
674	30.2739	75.4492	14.963	1.707	2.588 ± 0.036	0.261 ± 0.038	-31.57 ± 3.86	0.235 ± 0.023	99.67

7. Kinematics and Orbital parameters of Be 8

Five likely members with Gaia DR2 radial velocities (Table 5) allow us to calculate heliocentric velocities, (U , V , W) from the algorithm of Johnson and Soderblom (1987) [32]. These five members seem to be giant candidates according to their V and $(B - V)$ values (left panel of Figure 8). The calculated U , V , W velocities have been transformed to the components U' , V' , W' by correcting for the Solar motion $(U, V, W)_{\odot} = (+11.10, +12.24, +7.25) \text{ km s}^{-1}$ with respect to the local standard of rest (LSR) [33]. We adopt $R_{\odot} = 8.2 \pm 0.1 \text{ kpc}$ [34] and $V_{LSR} = 239 \text{ km s}^{-1}$ [35]. We adopt the right-hand system for the estimations. Their estimated heliocentric cartesian distances (x' , y' , z') (kpc) and LRS-velocity components (U' , V' , W') have been transformed to Galactic Rest of Frame (GSR) i.e., (x , y , z) (kpc) and (V_x , V_y , V_z) via the equations given by Kephley et al. (2007) [36]. The Galactocentric velocity component (V_{Φ}) (km s^{-1}) (or azimuthal velocity) in a cylindrical frame is estimated via $V_{\Phi} = \frac{xV_y - yV_x}{R}$. $V_{\Phi} < 0$ means prograde. Thus, the obtained kinematic parameters (U , V , W , V_{Φ}) km s^{-1} are listed in Cols. 2 – 5 of Table 6.

By utilising the "MWPotential2014" code in the galpy-code library¹ written by Bovy (2015) [37], peri- and apo-galactic distances (R_{\min} , R_{\max}) (kpc) and the maximum height distance (z_{\max}) (kpc) have been obtained. The orbital eccentricity (ecc) is estimated via the relation $e = (R_{\max} - R_{\min}) / (R_{\max} + R_{\min})$. Mean orbital radius (R_m) (kpc) is given as the mean of R_{\min} and R_{\max} distances. Each member's orbit has been integrated for 2.8 Gyr (Table 4) within the Galactic potential. The galactic potential is a sum of the Galactic components, as given in the paper of Bovy (2015) [37].

The orbital angular momentum components J_x , J_y , J_z and J_{\perp} (kpc km s^{-1}) for five members are calculated from the equations of Kephley et al. (2007) [36]. These orbital and angular momentum parameters (J_z , J_{\perp}) are given in Cols. 6–12 of Table 6. The total angular momentum J_{\perp} is defined as $J_{\perp} = (J_x^2 + J_y^2)^{1/2}$. For example, the right handed J_z value of a star near the Sun is $-1960 \text{ kpc km s}^{-1}$ from the solar values of R_{\odot} and V_{LSR} .

The vertical heliocentric velocities of $W = [12, 15] \text{ km s}^{-1}$ and azimuthal velocities, $V_{\Phi} = [-183, -197] \text{ km s}^{-1}$ of these five likely members indicate that they have typical Galactic disk velocities. They reside in outer Galactic disk, $R_m > 8.5 \text{ kpc}$ with the circular orbits, $\text{ecc} = [0.23, 0.30]$. Their Galactic heights reach to $z_{\max} = 1.27 \text{ kpc}$. According to Figure 13 of Carney et al. (1996) [38], thin and thick disk stars have the

¹<http://github.com/jobovy/galpy> [accessed 20 May 2019]

Table 6. For five probable members of Be 8, kinematics (U , V , W , V_Φ) km s^{-1} (Cols. 2–5) and orbital parameters (R_{max} , R_{min} , R_m , z_{max} (kpc)) and ecc (Cols. 6–10). Their orbital angular momentum values (J_z and J_\perp) (kpc km s^{-1}) (Cols. 11 – 12).

STAR-ID	U	V	W	V_Φ	R_{max}	R_{min}	R_m	z_{max}	ecc	J_z	J_\perp
508	-19.77	-55.89	15.36	-184.42	12.44	6.69	9.56	1.27	0.30	-2056.63	259.33
862	-14.94	-49.42	13.32	-192.93	12.12	7.09	9.60	1.15	0.26	-2106.96	242.69
737	-10.64	-48.43	11.61	-196.75	11.32	7.10	9.21	0.97	0.23	-2060.68	218.84
299	-9.91	-51.27	12.69	-193.21	11.66	7.07	9.37	1.07	0.24	-2076.34	235.59
674	-17.44	-57.54	11.64	-183.29	12.40	6.68	9.54	1.21	0.30	-2054.53	233.05

orbital eccentricities with $ecc < [0.25, 0.30]$ (circular orbits) and $0.30 < ecc < 0.45$ (elliptical). In the sense their orbital parameters reflect the properties of the Galactic thin disc. This is also consistent with what is expected of its metal content, $[M/H] = -0.27$.

The Galactic orbits of five probable members of Be 8 are presented in Figure 11(a) and (b). Five likely members with the circular orbits move from ~ 12 kpc to ~ 7 kpc on $x - y$ (kpc) (panel a). On $z - R$ (kpc) (panel b), they reach to $z \sim 1.3$ kpc for the range of $6 < R < 12$ kpc. Here R means the Galactocentric distance. The angular momenta (J_\perp , J_z) of these members fall in the range of $220 < J_\perp < 262$ kpc km s^{-1} for $-2107 \leq J_z \leq -2054$ kpc km s^{-1} . Their kinematics, dynamical and angular momentum values imply the indicators of Galactic thin disk population, according to fig. 11 of Kepley et al. (2007) [36].

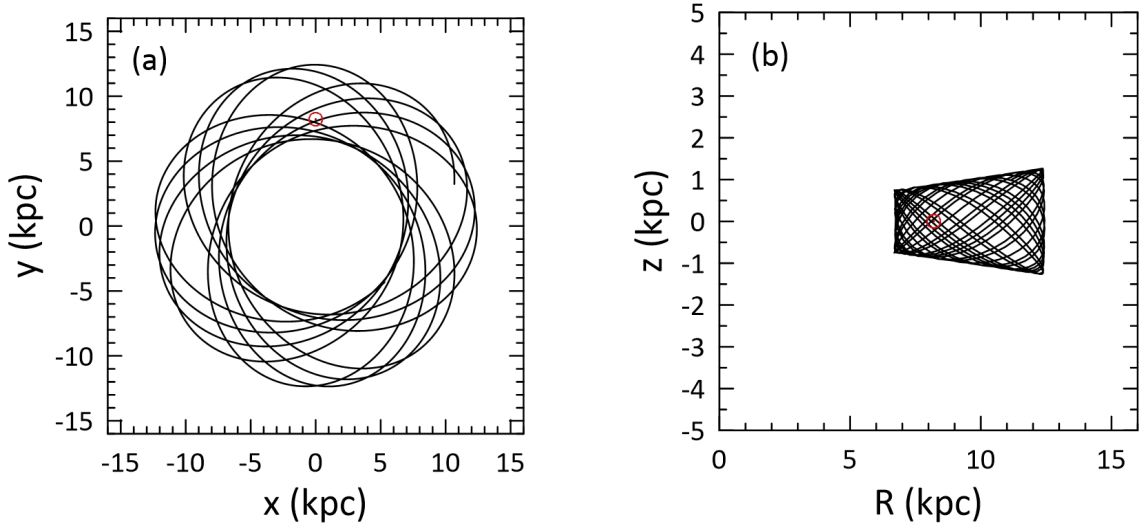


Figure 11. The orbits of five probable members of Be 8 on $x - y$ (kpc) (panel a) and $z - R$ (kpc) (panel b). Large circle denotes the position of the Sun, $(z_\odot, R_\odot) = (0, 8.2 \text{ kpc})$.

8. Discussions and Conclusions

For the cluster members of Be 8, the reddenings $E(B - V) = 0.69 \pm 0.03$ and $E(V - I) = 0.87 \pm 0.10$ have been obtained from $V - (B - V)$ and $V - (V - I)$ diagrams (Figure 8). These values are in good concordant

with the ones of $E(B - V) = 0.75$ and $E(V - I) = 0.88$, given by Hasegawa et al. (2004) [1]. Our $E(B - V)$ value is larger than 0.41 value given by Bukowiecki et al. (2001) [2] for 2MASS JHK_s photometry.

Our distance modulus and distance from $V - (B - V)$ are $(V_0 - M_V, d(\text{pc})) = (12.66 \pm 0.19, 3410 \pm 300 \text{ pc})$, which are in good agreement with the value (12.49, 3148 pc) of Hasegawa et al. (2004) [1]. Our value is somewhat smaller than the value (13.34, 3960 pc) of Bukowiecki et al. (2001) [2]. Our distance modulus/distance (pc) and age (Gyr) from $G - (G_{BP} - G_{RP})$ are in quite compatible with the ones of the colour indices, $(B - V)$, $(V - I)$ and $(R - I)$ (Table 4). The median Gaia DR2 parallax from 43 likely members ($\sigma_\varpi/\varpi < 0.20$) gives us $\varpi = 0.272 \pm 0.060 \text{ mas}$ which corresponds to $d = 3676 \pm 810 \text{ pc}$. This distance is in good concordance with the photometric distances (3410–3620 pc) within the uncertainties (Table 4). A global systematic offset of Gaia DR2 parallaxes is $\Delta\varpi = -0.029 \text{ mas}$ in terms of an inertial reference frame, derived by Lindegren et al. (2018) [4]. Recent values for the zero point shift of parallax have been found as $\Delta\varpi = -0.045 \pm 0.009 \text{ mas}$ [39], $\Delta\varpi = -0.053 \pm 0.003 \text{ mas}$ [40], and $\Delta\varpi = -0.046 \pm 0.013 \text{ mas}$ [41], respectively. A correction of 0.005 mas to the median value of our median parallax gives a closer distance with a difference of 66 pc for Be 8.

The age of Be 8 is $2.80 \pm 0.20 \text{ Gyr}$ and this is younger than 3.16 Gyr of Hasegawa et al. (2004) [1] and Bukowiecki et al. (2001) [2]. Its MAI age ($A = 2.94 \text{ Gyr}$) is in concordant with its isochrone age. Discrepancies of the distance moduli, distances and ages as compared to the literature stem from the usage of different heavy element abundances, isochrones, reddenings and photometries such as 2MASS JHK_s, as mentioned by Moitinho (2010) [42].

Two BS candidates reside in core radius of $1.8'$ of Be 8 (Figure 10). BS stars potentially locate in the inner regions of stellar clusters [43]. According to Ferraro (2016) [44], their formation ways are explained: mass transfer in binary systems [45] due to the merging of the two stars and stellar collisions [46].

It is surprising to find Be 8 with $[M/H] = -0.27$ (close to solar metallicity) at such large galactic radius ($R = 10.57 \text{ kpc}$). However, the orbits in Fig.11(a) and (b) show that the cluster passed a part of its time at galactocentric radius, $R = 6 - 7 \text{ kpc}$, and then possibly it was born at that radius, which would explain the metallicity. According to Figure 3 – 4 ($[M/H]$ versus R (kpc)) of Lepine et al. (2011) [47], Be 8 with $[M/H] = -0.27$ and $R = 10.57 \text{ kpc}$ reside in a region of $R > 9 \text{ kpc}$ (co-rotation gap at 9 kpc). In the sense it may have been originating from different galactic radius or different star formation region [47].

Acknowledgements

We wish to thank the staff of Sierra Nevada Observatory, Granada-Spain. RM acknowledge the financial support from the UNAM under DGAPA grant PAPIIT IN100918. We thank J. Lepine for his valuable comments. This paper has made use of results from the European Space Agency (ESA) space mission Gaia, the data from which were processed by the Gaia Data Processing and Analysis Consortium (DPAC). Funding for the DPAC has been provided by national institutions, in particular the institutions participating in the Gaia Multilateral Agreement. The website of Gaia mission is <http://www.cosmos.esa.int/gaia>.

References

- [1] Hasegawa T, Malasan HL, Hideyo KH, Obayashi H, Kurabayashi T et al. New Photometric Data of Old Open Clusters in the Anti-Galactic Center Region. Pub. Astron. Soc. Japan 2004; 56: 295. doi: 10.1093/pasj/56.2.295

- [2] Bukowiecki L, Maciejewski G, Konorski P, Strobel A. Open Clusters in 2MASS Photometry. I. Structural and Basic Astrophysical Parameters. *Acta Astronomica* 2011; 61: 231-246. [ACTA AST](#).
- [3] Mermilliod JC. The database for stars in open clusters. II. A progress report on the introduction of new data. *Bull. Inform. CDS* 1992; 40: 115 [NASA ADS](#)
- [4] Lindegren L, Hernandez J, Bombrun A, Klioner S, Bastian U et al. Gaia Data Release 2. The astrometric solution. *Astron. Astrophys.* 2018; 616: A2. doi: 10.1051/0004-6361/201832727
- [5] Brown AGA, Vallenari A, Prusti T, de Bruijne JHJ, Babusiaux C et al. Gaia Data Release 2. Summary of the contents and survey properties. *Astron. Astrophys.* 2018; 616: A1. doi: 10.1051/0004-6361/201833051
- [6] Balaguer-Nunez L, Tian KP, Zhao JL. Determination of proper motions and membership of the open clusters NGC 1817 and NGC 1807. *Astron. Astrophys. Suppl.* 1998; 133: 387. doi: 10.1051/aas:1998324
- [7] Sariya DP, Yadav RKS, Bellini A. Proper motions and membership probabilities of stars in the region of globular cluster NGC 6809. *Astron. Astrophys.* 2012; 543: 87. doi: 10.1051/0004-6361/201219306
- [8] Dias WS, Monteiro H, Lepine JRD, Prates R, Gneiding CD et al. Astrometric and photometric study of Dias 4, Dias 6, and other five open clusters using ground-based and Gaia DR2 data. *Mon. Not. Roy. Astron. Soc.* 2018; 481: 3887. doi: 10.1093/mnras/sty2341
- [9] Roeser S, Demleitner M, Schilbach E. The PPMXL Catalog of Positions and Proper Motions on the ICRS. Combining USNO-B1.0 and the Two Micron All Sky Survey (2MASS). *Astron. J.* 2010; 139: 2440-2447. doi: 10.1088/0004-6256/139/6/2440
- [10] Skrutskie MF, Cutri R, Stiening R, Weinberg MD, Schneider SE et al. The Two Micron All Sky Survey (2MASS). *Astron. J.* 2006; 131: 1163-1183 doi: 10.1086/498708
- [11] Cantat-Gaudin T, Jordi C, Vallenari A, Bragaglia A, Balaguer-Nunez L et al. A Gaia DR2 view of the Open Cluster population in the Milky Way. *Astron. Astrophys.* 2018; 618: 93. doi: 10.1051/0004-6361/201833476
- [12] Zacharias N, Finch CT, Girard TM, Henden A, Bartlett JL et al. The Fourth US Naval Observatory CCD Astrograph Catalog (UCAC4). *Astron. J.* 2013; 145: 44. doi: 10.1088/0004-6256/145/2/44
- [13] Landolt AU. UBVRI Photometric Standard Stars Around the Celestial Equator: Updates and Additions. *Astron. J.* 2009; 137: 4186-4269. doi: 10.1088/0004-6256/137/5/4186
- [14] van Dokkum PG. Cosmic-Ray Rejection by Laplacian Edge Detection. *Pub. Astron. Soc. Pac.* 2001; 113: 1420-1427. doi: 10.1086/323894
- [15] Cutri RM, Wright EL, Conrow T, Fowler JW, Eisenhardt PRM et al. VizieR Online Data Catalog: AllWISE Data Release (Cutri+ 2013). *VizieR On-line Data Catalog: II/328.* 2013; 2328: 0C. [WISE](#)
- [16] Akkaya İ, Schuster WJ, Michel R, Chavarría-K C, Moitinho A et al. CCD UBVRI Photometry of the Galactic open clusters: Be 89, Ru 135, and Be 10. *Rev. Mex. Astron. Astrofis* 2010; 46: 385.
- [17] Akkaya Oralhan I, Karataş Y, Schuster WJ, Michel R, Chavarría-K C. CCD UBV(RI)(C) photometry of twenty open clusters. *New Astronomy* 2015; 34: 195. doi: 10.1016/j.newast.2014.06.011
- [18] Bonatto CH, Bica E. Old open clusters in the inner Galaxy: FSR1744, FSR89 and FSR31. *Astron. Astrophys.* 2007; 473: 445. doi: 10.1051/0004-6361:20077675
- [19] King IR. The structure of star clusters. III. Some simple dynamical models. *Astron. J.* 1966; 71: 64. doi: 10.1086/109857
- [20] Pedregosa F, Varoquaux G, Gramfort A, Michel V, Thirion B et al. Scikit-learn: Machine Learning in Python, *The Journal of Machine Learning Research* 2011; 12: 2825-2830 [JMLR](#)
- [21] Wu ZY, Tian KP, Balaguer-Nunez L, Jordi C, Zhao JL et al. Determination of proper motions and membership of the open star cluster NGC 2548. *Astron. Astrophys.* 2002; 381: 464. doi: 10.1051/0004-6361:20011474

- [22] Schmidt-Kaler Th. in Landolt-Bornstein, Numerical Data and Functional Relationships in Science and Technology, New Series, Group VI, Vol2b, ed. K Schaifers & H H Voigt, p.14. Springer Verlag, Berlin 1982.
- [23] Karataş Y, Schuster WJ. Metallicity and absolute magnitude calibrations for UBV photometry. Mon. Not. Roy. Astron. Soc. 2006; 371: 1793. doi: 10.1111/j.1365-2966.2006.10800.x
- [24] Bressan A, Marigo P, Girardi L, Salasnich B, Dal Cero C et al. PARSEC: stellar tracks and isochrones with the PAdova and TRieste Stellar Evolution Code. Mon. Not. Roy. Astron. Soc. 2012; 427: 127. doi: 10.1111/j.1365-2966.2012.21948.x
- [25] Güneş O, Karataş Y, Bonatto C. A dynamical evolution study of 40 2MASS open clusters. Astron. Nachr. 2017; 338: 464. doi: 10.1002/asna.201712978
- [26] Dean JF, Warren PR, Cousins AWJ. Reddenings of Cepheids using BVI photometry. Mon. Not. Roy. Astron. Soc. 1978; 183: 569. doi: 10.1093/mnras/183.4.569
- [27] Mathis J. Interstellar dust and extinction. Annu. Rev. Astron. Astrophys. 1990; 28: 37. doi: 10.1146/annurev.aa.28.090190.000345
- [28] Straizys V. Multicolor Stellar Photometry, Astronomy and Astrophysics Series, Vol 15, ed A G Pacholczyk, Tucson, Arizona: Pachart Pub. House 1995.
- [29] Bragaglia A, Fu X, Mucciarelli A, Andreuzzi G, Donati P. The chemical composition of the oldest nearby open cluster Ruprecht 147. Astron. Astrophys. 2018; 619: A176. doi: 10.1051/0004-6361/201833888
- [30] Phelps RL, Janes KA, Montgomery KA. Development of the Galactic Disk: A Search for the Oldest Open Cluster. Astron. J. 1994; 107: 1079. doi: 10.1086/116920
- [31] Salaris M, Weiss A, Percival SM. The age of the oldest Open Clusters. Astron. Astrophys. 2004; 414: 163. doi: 10.1051/0004-6361:20031578
- [32] Johnson DRH, Soderblom DR. Calculating galactic space velocities and their uncertainties, with an application to the Ursa Major group. Astron. J. 1987; 93: 864. doi: 10.1086/114370
- [33] Schönrich R, Binney J, Dehnen W. Local Kinematics and the Local Standard of Rest. Mon. Not. Roy. Astron. Soc. 2010; 403: 1829. doi: 10.1111/j.1365-2966.2010.16253.x
- [34] Bland-Hawthorn J, Gerhard O. The Galaxy in Context: Structural, Kinematic and Integrated Properties. Annu. Rev. Astron. Astrophys. 2016; 54: 529. doi: 10.1146/annurev-astro-081915-023441
- [35] Brunthaler A, Reid MJ, Menten KM, Zheng XW, Bartkiewicz A et al. The Bar and Spiral Structure Legacy (BeSSeL) survey: Mapping the Milky Way with VLBI astrometry. Astron. Nachr. 2011; 332(No5): 461. doi: 10.1002/asna.201111560
- [36] Kewley A, Morrison HL, Helmi A, Kinman TD, van Deyne J et al. Halo Star Streams in the Solar Neighborhood. Astron. J. 2007; 134: 1579. doi: 10.1086/521429
- [37] Bovy J. galpy: A python LIBRARY FOR GALACTIC DYNAMICS. Astron. Astrophys. Suppl. 2015; 216: 29. doi: 10.1088/0067-0049/216/2/29
- [38] Carney BW, Laird JB, Latham DW, Aguilar LA. A Survey of Proper Motion Stars. XIII. The Halo Population. Astron. J. 1996; 112: 668. doi: 10.1086/118042
- [39] Yalçınova LN, Chemel AA, Glushkova EV, Dambis AK, Klinichev AD. A Comprehensive Study of 94 Open Clusters Based on the Data from IPHAS, GAIA DR2, and Other Sky Surveys. Astrophys. Bull. 2018; 73: 335. doi: 10.1134/S1990341318030070
- [40] Zinn JC, Pinsonneault MH, Huber D, Stello D. Confirmation of the Gaia DR2 parallax zero-point offset using asteroseismology and spectroscopy in the Kepler field. Astron. J. 2018; 878: 1538-4357. doi: 10.3847/1538-4357/ab1f66
- [41] Riess AG, Casertano S, Yuan W, Macri L, Bucciarelli B et al. Milky Way Cepheid Standards for Measuring Cosmic Distances and Application to Gaia DR2: Implications for the Hubble Constant. Astron. J. 2018; 861: 126. doi: 10.3847/1538-4357/aac82e

- [42] Moitinho A. Star clusters: basic galactic building blocks, Proceedings IAU Symposium No266, ed. Rde Grijs and JRD Lepine 2010.
- [43] Carney B. Star Clusters, Saas-Fee Advanced Course 28, Lecture Notes 1998, Swiss Society for Astrophysics and Astronomy, ed. L Labhardt and B Binggeli, p.1-222. Springer-Verlag Berlin 2001.
- [44] Ferraro FR. IAUS-Star Clusters and Black Holes in Galaxies across Cosmic Time, Proceedings of the International Astronomical Union, IAU Symposium. 2016; 312: 171-180
- [45] McCrea WH. Extended main-sequence of some stellar clusters. Mon. Not. Roy. Astron. Soc. 1964; 128: 147. doi: 10.1093/mnras/128.2.147
- [46] Hills J, Day C. Stellar Collisions in Globular Clusters. Astrophysical Letters 1976; 17: L87. [NASA ADS](#)
- [47] Lepine JRD, Cruz P, Scarano S, Barros DA, Dias WS et al. Overlapping abundance gradients and azimuthal gradients related to the spiral structure of the Galaxy. Mon. Not. Roy. Astron. Soc. 2011; 417: 698. doi: 10.1111/j.1365-2966.2011.19314.x